Agglomerate-free BaTiO$_3$ particles by salt-assisted spray pyrolysis

Yoshifumi Itoh and I. Wuled Lenggoro
*Department of Chemical Engineering, Graduate School of Engineering, Hiroshima University,
Higashi-Hiroshima 739-8527, Japan*

Sotiris E. Pratsinis
*Department of Mechanical and Process Engineering, Swiss Federal Institute of Technology (ETH),
ETH Zurich, Zurich, CH-8092, Switzerland*

Kikuo Okuyama[a)]
*Department of Chemical Engineering, Graduate School of Engineering, Hiroshima University,
Higashi-Hiroshima 739-8527, Japan*

Optimum conditions for the synthesis of nonagglomerated BaTiO$_3$ particles by
salt-assisted spray pyrolysis (SASP) were investigated. The effect of particle residence
time in the reactor and salt concentration on the crystallinity and surface morphology
of BaTiO$_3$ was examined by x-ray diffraction and scanning electron microscopy.
Mixtures of a metal chloride or nitrate salt, dissolved in aqueous precursor solutions,
were sprayed by an ultrasonic atomizer into a five-zone hot-wall reactor. By
increasing the salt concentration or the particle residence time in the hot zone, the
primary particle size was increased, and its surface texture was improved compared
to BaTiO$_3$ particles prepared by conventional spray pyrolysis. The SASP-prepared
BaTiO$_3$ crystal was transformed from cubic to tetragonal by simply increasing the salt
concentration at constant temperature and residence time. Further thermal treatments
such as calcination or annealing are not necessary to obtain nonagglomerated
tetragonal BaTiO$_3$ (200–500 nm) particles with a narrow size distribution. Increasing
the carrier gas flow rate and decreasing the residence time in the hot zone resulted in
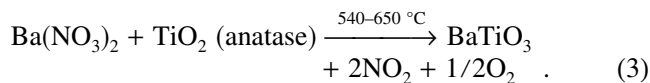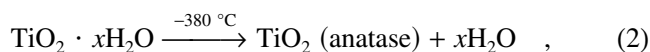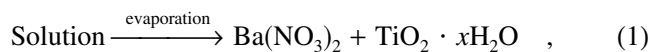cubic BaTiO$_3$ particles about 20 nm in diameter.

I. INTRODUCTION

Barium titanate has many applications, most notably for piezoactuators and multilayer ceramic capacitors, as the result of its excellent dielectric, ferroelectric, and piezoelectric properties. Tetragonal barium titanate is used in electronic devices for its ferroelectric properties, and its cubic phase has a high dielectric constant, thus making it suitable for use in capacitors.[1] The dielectric constant and crystal structure are dependent on the grain size of the particles. Arlt *et al.* reported that the maximum dielectric constant for pure BaTiO$_3$ ceramics is realized at a grain size of 0.8 μm.[2] Sakabe *et al.* prepared tetragonal BaTiO$_3$ particles as small as 70 nm by hydrolysis of Ba(OH)$_2$ and Ti-alkoxide.[3] Kajiyoshi *et al.*[4] and Dutta and Gregg[5] reported that the critical particle size of the tetragonal structure is in excess of 100 nm. Cho *et al.* reported that BaTiO$_3$ particles prepared from organic precursors are in the tetragonal phase when they are larger than 20 nm.[6]

Several routes for the synthesis of BaTiO$_3$ particles, including coprecipitation,[7] sol-gel, hydrothermal synthesis,[1] and mechanochemical[8] techniques have been reported. Hydrothermal and solid-state processes are used commercially for the preparation of BaTiO$_3$ powder because of their low cost and ease of production. In solid-state synthesis, BaCO$_3$, TiO$_2$ and other additives are mechanically milled and calcined at a high temperature to permit solid-state reactions.[8] Hydrothermal processing can be used to prepare tetragonal BaTiO$_3$ particles with an average particle size of 80 nm at 240 °C for 12 h.[9] The disadvantages of these processes include inhomogeneous chemical composition, strong agglomeration, a rather poor morphology, and difficulties in controlling crystal size. A surface modifier is necessary to prevent agglomeration of the nanoparticles.[10] Controlling the composition of the resulting BaTiO$_3$ particles remains difficult because Ba ions tend to be lost during washing. As a result, an excess of barium precursor must be used, and the conversion reaction conducted in an argon atmosphere using CO$_2$-free water to obtain high-purity barium titanate.[11] Furthermore, several hours are required to produce homogeneous and highly crystalline particles using hydrothermal and mechanochemical processes.[1,8–10]

[a)]Address all correspondence to this author.
  e-mail: okuyama@hiroshima-u.ac.jp

Spray pyrolysis is widely known to be a continuous, single-step preparation method for the production of fine homogeneous and multicomponent powders. Milosevic *et al.* reported on the production of spherical BaTiO₃ powders by spray pyrolysis at 700 and 900 °C of ethanol/water solutions of $BaCl_2$ and $TiCl_4$ that were suspended using two-fluid and ultrasonic atomizers.[12] Ogihara *et al.* successfully synthesized chemically homogeneous, fine, and spherical particles of BaTiO₃ from a nitric acid solution of $Ba(CH_3COO)_2$ and $Ti(OC_3H_7)_4$.[13] Nonaka *et al.* reported that replacing part of the precursor solution of titanium tetraisopropoxide (TTIP) and $Ba(NO_3)_2$ or $Sr(NO_3)_2$ in dilute nitric acid with alcohols and hydrogen peroxide improved the chemical homogeneity of the products and reduced the amount of by-products during the synthesis of BaTiO₃ and SrTiO₃ particles by spray pyrolysis, as evidenced by thermogravimetric differential thermal analysis.[14] They proposed that the formation of BaTiO₃ proceeds as follows:

$$\text{Solution} \xrightarrow{\text{evaporation}} Ba(NO_3)_2 + TiO_2 \cdot xH_2O \quad , \qquad (1)$$

$$TiO_2 \cdot xH_2O \xrightarrow{-380\ °C} TiO_2 \text{ (anatase)} + xH_2O \quad , \qquad (2)$$

$$Ba(NO_3)_2 + TiO_2 \text{ (anatase)} \xrightarrow{540-650\ °C} BaTiO_3 \\ + 2NO_2 + 1/2O_2 \quad . \qquad (3)$$

Although the synthesis temperature is sufficient for the formation of tetragonal BaTiO₃ particles at 700 °C,[13,14] residual materials, such as $BaCO_3$, were coproduced at temperatures under 900 °C.[15] Conventional spray pyrolysis results in multiple nano-sized crystallites that are virtually inseparable, since they form a three-dimensional network.

Xia *et al.* reported that the presence of a salt in the precursor solution drastically inhibited the agglomeration of nanocrystallites.[16] These salts remain on the particle surface and hinder the bonding of nanocrystallites. The salts can be easily removed by washing. Xia *et al.* demonstrated the feasibility of this method, salt-assisted spray pyrolysis (SASP),[16] by producing Y_2O_3–ZrO_2, ZnS, CeO_2,[17] and NiO[18] nanoparticles (below 100 nm) by the spray pyrolysis of eutectic mixtures of salts such as metal chlorides or nitrates in an aqueous precursor solution. SASP requires no further thermal treatment of the product, such as calcination or annealing, because the metal salts enhance the homogeneity of the crystals and crystal growth. For this paper, the effect of salt concentration and droplet/particle residence time in hot zone on the crystallinity, morphology, and size of SASP-prepared BaTiO₃ particles was examined.

II. EXPERIMENTAL

Precursor solutions were prepared by dissolving a stoichiometric ratio of $Ba(NO_3)_2$ (99.0%) and $Ti(OC_3H_7)_4$ (97.0%) in dilute 1 mol/l nitric acid.[14] The concentration was set from 0.01 to 0.05 mol/l of BaTiO₃, while the Ba/Ti ratio of the precursor solutions was 1.00 for all experiments. Solutions of KNO_3 (99.0%) and $NaNO_3$ (99.0%) in molar ratio of 51:49 were added to the precursor solution with salt/Ti molar ratios of 0.0–50.0. All chemicals were purchased from Kanto Kagaku, Tokyo, Japan.

Figure 1 shows a schematic diagram of the apparatus. The precursor solution was sprayed by means of an ultrasonic aerosol atomizer (1.7 MHz) into a 1.3-cm inner diameter, 150-cm long Al_2O_3 ceramic tube heated by an electric furnace at 1000 °C with five independently controlled heating zones, each 20 cm in length. Nitrogen, at a flow rate of 1 l/min, unless otherwise stated, was used to carry the atomized aerosols into the furnace, resulting in a droplet/particle residence time of 1.6 s in hot zone. The resulting powders were collected by an electrostatic aerosol precipitator operated at 150 °C and 9 kV while the gasses were dried by a cold trap and a diffusion dryer and then neutralized by passage through a NaOH trap before being exhausted by a vacuum pump. To remove the salt, the collected particles were washed, centrifuged with ultra-pure water, and dried for 10 h at 50 °C in a muffle furnace after washing.

The crystalline phases were examined by x-ray diffraction (XRD; RINT 2200V, Rigaku Tokyo, Japan) with Cu K_α radiation recorded at 40 kV and 20 mA. The average size of the crystallites was estimated using Scherer's formula. The grain size and morphology of the particles were characterized by field-emission scanning electron microscopy (FE-SEM; S5000, Hitachi, Tokyo, Japan) operated at 20 kV. For scanning electron microscopy (SEM), the sample, suspended in ethanol, was sonicated and a few drops of the suspension deposited onto
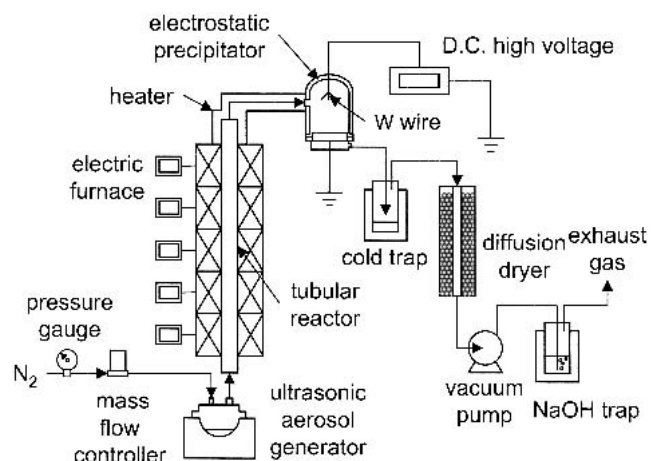

FIG. 1. Schematic diagram of the SASP apparatus.

the substrate, dried, and sputter-coated with Pt–Pd. The geometric mean diameter and geometrical standard deviation were determined by randomly sampling 300 particles from the SEM photographs.

III. RESULTS AND DISCUSSION

Figure 2 shows the XRD patterns of BaTiO$_3$ particles prepared by (a) conventional and (b–e) SASP at different salt concentrations. In addition, the standard XRD patterns of cubic[19] and tetragonal[20] phases of BaTiO$_3$ are also shown at the bottom of Fig. 2. The XRD pattern of hydrothermally[4,5] synthesized tetragonal BaTiO$_3$ (Toda Kogyo Corp., Hiroshima, Japan) is also shown in Fig. 2(f). All conventional spray pyrolysis (SP)-prepared particles show the presence of cubic BaTiO$_3$. All SASP-prepared samples have sharper peaks, indicating the presence of larger crystallites than the conventional SP sample. At a salt/Ti = 8 [Fig. 2(d)], there are split peaks at 2θ of 45° and 66°, implying the presence of tetragonal
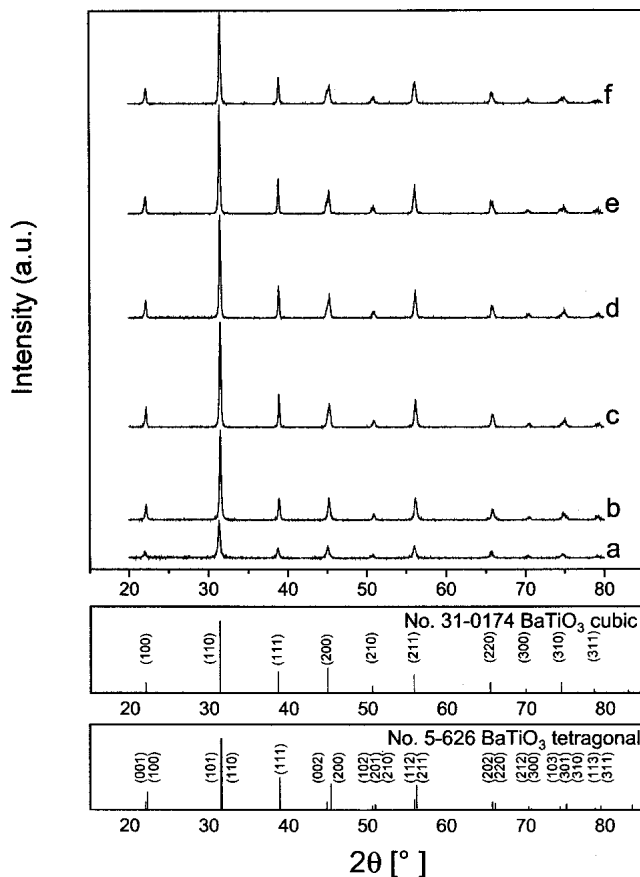
BaTiO$_3$. This phase transition behavior is illustrated more clearly in Fig. 3 where the transition from the cubic [Figs. 3(a) and 3(b)] to the ferroelectric tetragonal barium titanate [Figs. 3(d) and 3(e)] is associated with increasing the salt/Ti molar ratio. At a salt/Ti ratio = 4 [Fig. 3(c)], the diffraction peak at 2θ around 45° slightly widens, which can be indicative of a peak split. However, it is still difficult to distinguish the (002) and (200) planes, since they overlap. The other split peaks of the tetragonal phase were observed at 2θ around 66° [Fig. 3(c)]. A further increase in the salt/Ti ratio to 15 [Fig. 3(e)] results in the easier identification of the diffraction peaks. The amount of tetragonal BaTiO$_3$ increases with increasing salt/Ti ratios, indicating that the SASP procedure not only enhances the crystallinity but also controls the phase composition through the salt/Ti ratio at the same pyrolysis temperature.

Figure 4 shows FE-SEM images of the effect of salt concentration on the morphology of BaTiO$_3$ particles for a precursor solution concentration of (a–d) 0.05 mol/l and (e) 0.01 mol/l. For reference, a FE-SEM image of hydrothermally prepared BaTiO$_3$ is also shown in Fig. 4(f). The particles prepared without salt [Fig. 4(a)] are spherical with a rough, cauliflowerlike surface.

FIG. 2. XRD patterns of BaTiO$_3$ particles prepared with 0.05 mol/l precursor solutions at 1000 °C by (a) conventional spray pyrolysis and (b) SASP at salt/Ti ratios of 1, (c) 4, (d) 8 and (e) 15 of BaTiO$_3$ made with 0.05 mol/l precursor solutions, (f) hydrothermally synthesized BaTiO$_3$.
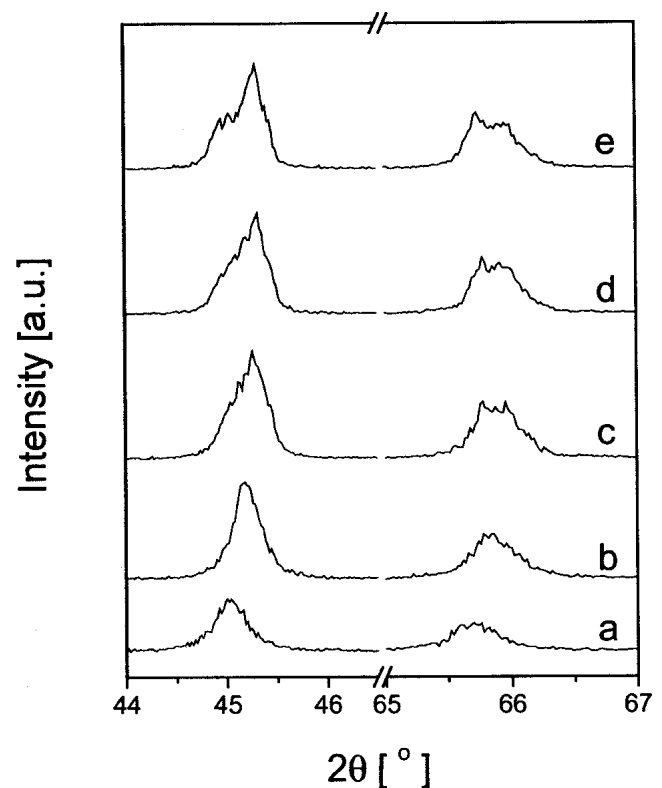

FIG. 3. Enlarged XRD pattern around 2θ = 45 and 65° of (a) conventional spray pyrolysis, and (b) SASP at salt/Ti ratios of 1, (c) 4, (d) 8, and (e) 15 of BaTiO$_3$ made with 0.05 mol/l precursor solutions.
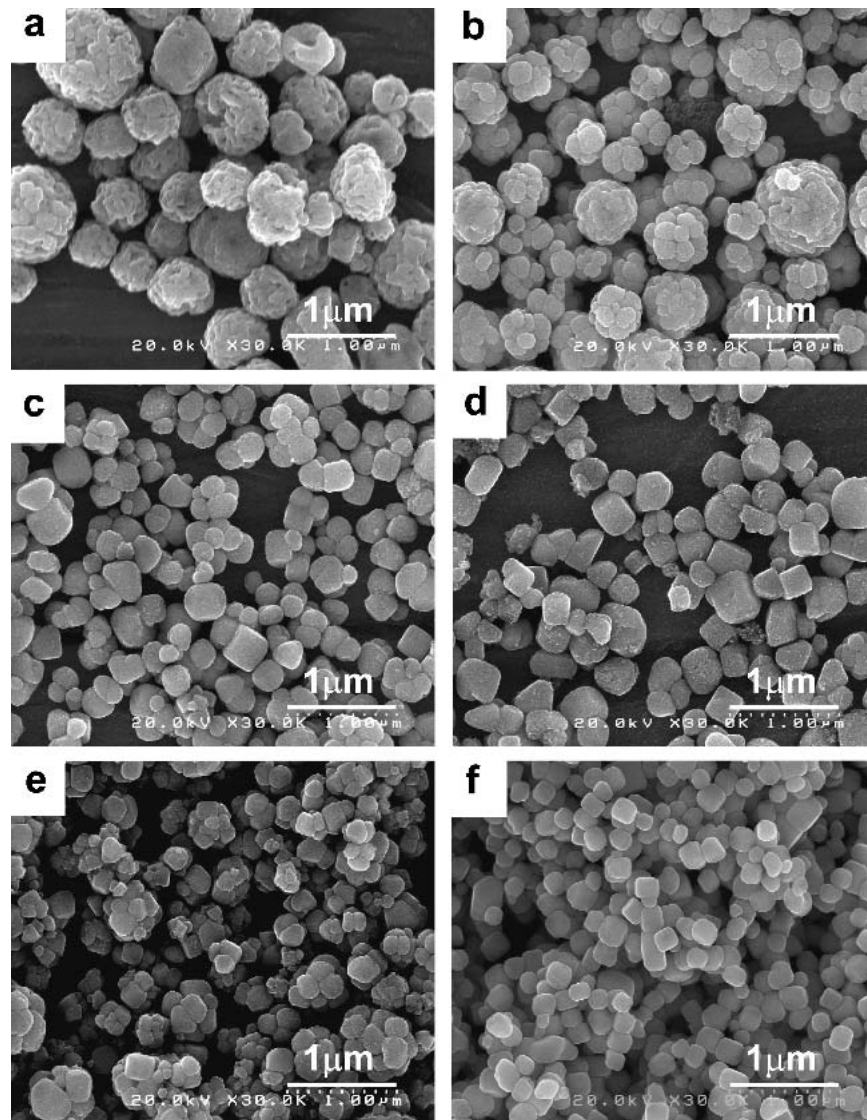
FIG. 4. FE-SEM images of SASP-made BaTiO$_3$ particles prepared at different salt/Ti ratios: (a) 0, (b) 4, (c) 8, (d) 15 and (e) 20. Precursor solutions 0.05 mol/l for (a–d) and 0.01 mol/l for (e). The SEM image of hydrothermally made BaTiO$_3$f).

Particles at low salt/Ti ratios [Fig. 4(b)] were agglomerates of a few crystallites with smooth surface and well-defined grain boundaries sharper than those shown in Fig. 4(a). At a higher salt/Ti ratio [Fig. 4(c) or 4(d)], the degree of agglomeration decreased, resulting in nearly nonagglomerated, crystalline particles. The primary particle size increases with increasing salt concentration. The particles shown in Fig. 4(e) were prepared by decreasing the concentration of BaTiO$_3$ from 0.05 [Fig. 4(b)] to 0.01 mol/l while maintaining the salt concentration at 0.20 mol/l, resulting in a geometric mean particle diameter of 310 nm with agglomerated small primary particles. Compared to Fig. 4(b), the primary particles [Fig. 4(e)] seemed smaller than those of Fig. 4(b). The geometric mean diameter and the standard deviation of these primary particles were determined to be 118.5 nm and 1.52, respectively.

Figure 5 shows the size distributions of the BaTiO$_3$ particles of Figs. 4(a)–4(d). The white bars [Figs. 5(b) and 5(c)] refer to the primary particle size distribution while the black ones refer to the agglomerated particle size distribution. The inset values show the geometric mean diameter and standard deviation of the primary and agglomerated particles respectively, as calculated from the particle SEM Feret diameters. When the salt/Ti ratio was increased, the agglomerated particle size tended to decrease, but the primary particle size and crystallinity of BaTiO$_3$ increased. Decreasing the precursor concentration led to a decrease in the primary particle size and crystallinity, as discussed above. Thus, the degree of crystallization is affected not only by the pyrolysis temperature and processing time, but also the solution composition and salt concentration. This implies an optimum salt concentration exists for forming well-crystallized particles.
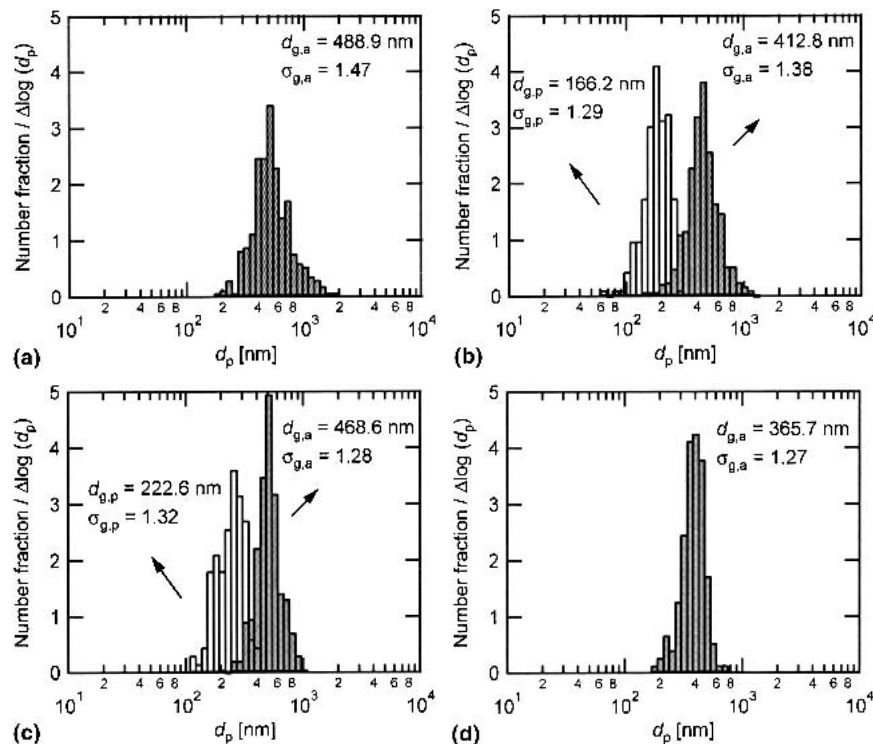
FIG. 5. Particle size distributions of BaTiO₃ particles prepared by SASP at a precursor concentration 0.05 mol/l and salt/Ti ratio (a) 0, (b) 4, (c) 8, and (d) 15.

Figure 6 shows FE-SEM images of the effect of droplet/particle residence time in the hot zone on the morphology of BaTiO₃ particles by changing the furnace length [Figs. 6(a)–6(c)] through the number of 20-cm heating zones used or the carrier gas flow rate [Figs. 6(b), 6(d), and 6(e)] at 1000 °C. The solution concentration for BaTiO₃ particles was 0.05 mol/l [Figs. 6(a)–6(e)] and 0.01 mol/l [Figs. 6(f) and 6(g)]. The salt/Ti ratios were 4 [Figs. 6(a)–6(e)] and 15 [Figs. 6(f) and 6(g)]. When the furnace length was increased from 20 to 40 and 100 cm, the size of primary particles increased. When the carrier gas flow rate increased from 1 l/min to 5 l/min at a furnace length of 40 cm, the primary particle size decreased, and even a few single primary particles were observed. A further increase in the carrier gas flow rate to 10 l/min [Fig. 6(e)] resulted in very small crystallites agglomerated inside a shell-like crust, the size of which was proportional to the original droplet. At a precursor concentration at 0.01 mol/l and salt/Ti = 15, the primary particle size increased when the furnace length was increased from 20 cm [Fig. 6(f)] to 100 cm [Fig. 6(g)]. Regardless of the heating zone length, all particles in Fig. 6 were cubic BaTiO₃, even when the primary particle size was as small as 20 nm [Fig. 6(e)].

Figure 7 shows an illustration of the mechanism of BaTiO₃ particle formation by SASP, which consists of (i) TiO₂ · xH₂O, Ba(NO₃)₂ and salts precipitating from the solution as the solubility of the precipitates decreases by solvent evaporation; (ii) the mixture of KNO₃ and NaNO₃ melting at around 300 °C and intermediates such as Ba(NO₃)₂ and TiO₂ · xH₂O, which may be surrounded by the molten salt; (iii) the TiO₂ · xH₂O decomposing into TiO₂ (anatase) at temperatures up to 380 °C while Ba(NO₃)₂ decomposes at around 590 °C and reacts with TiO₂ at about 540 °C; (iv) newly formed BaTiO₃ growing initially from the liquid phase, and later, by sintering and densification. In the case of a high salt/Ti ratio [Fig. 7(a)], intermediate BaTiO₃ particles are surrounded by a sufficient amount of molten salt so the agglomeration of primary BaTiO₃ particles occurs by sintering and densification at long residence times. The sintered particles do not grow larger at a certain salt/Ti ratio. At short processing times such as those in Fig. 6(e) (10 l/min carrier gas flow rate, 40 cm reactor length), precipitates appear inside the droplet, since it is dried rapidly. These precipitates decompose and some undergo aggregation, resulting in agglomerated particles, but sintering is inhibited at these short residence times. During drying and solvent evaporation, the precipitates diffuse to the droplet surface. The precipitates then form a shell and decompose later on. In the case of low salt/Ti ratio [Fig. 7(b)], the crystallites can easily come into contact with each other because insufficient molten salt is not available to hinder the crystallite growth. As a result, agglomerated primary particles with a smooth surface are formed. In conclusion, molten salts enhance crystallization and
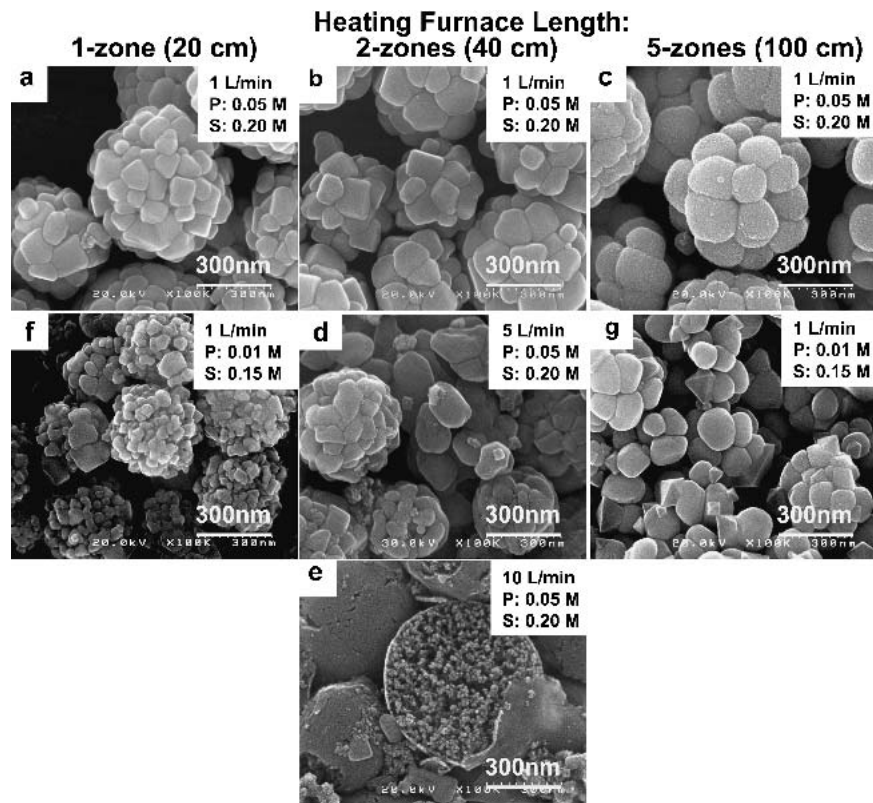
FIG. 6. Effect of the residence time on the morphology of BaTiO$_3$ particles; (a) 1 zone (20 cm), 1 l/min, solution concentration (P) = 0.05 mol/l, salt concentration (S) = 0.20 mol/l; (b) 2 zones (40 cm), 1 l/min, P = 0.05 mol/l, S = 0.20 mol/l; (c) 5 zones (100 cm), 1 l/min, P = 0.05 mol/l, S = 0.20 mol/l; (d) 2 zones, 5 l/min, P = 0.05 mol/l, S = 0.20 mol/l; (e) 2 zones, 10 l/min, P = 0.05 mol/l, S = 0.20 mol/l; (f) 1 zone, 1 l/min, P = 0.01 mol/l, S = 0.15 mol/l; (g) 5 zones, 1 l/min, P = 0.01, S = 0.15 mol/l.
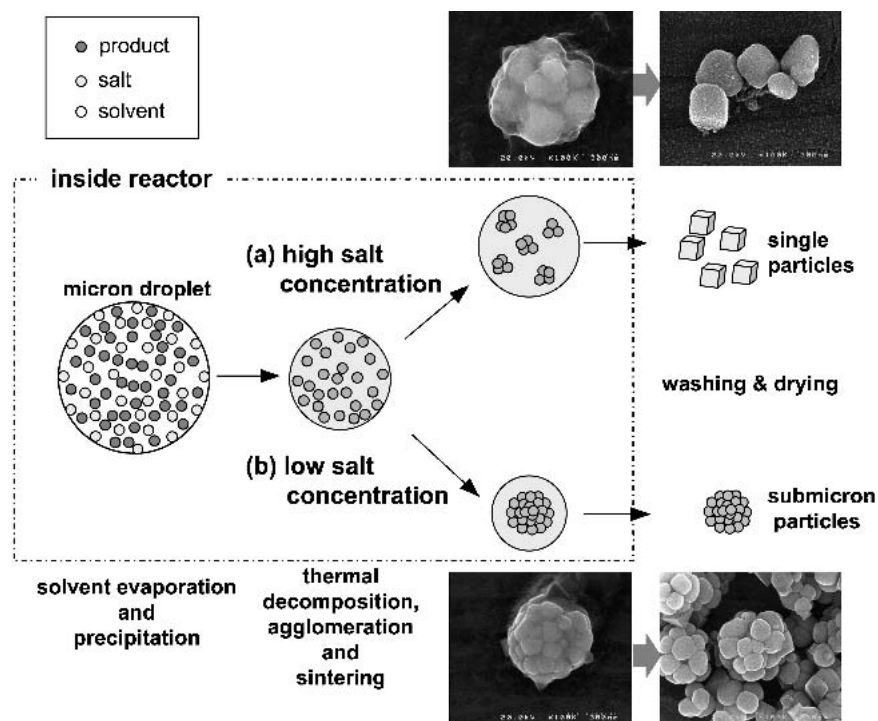

FIG. 7. Schematic illustration of the mechanism of BaTiO$_3$ particle formation by SASP. High salt concentrations favor the formation of large and nonagglomerated particles.
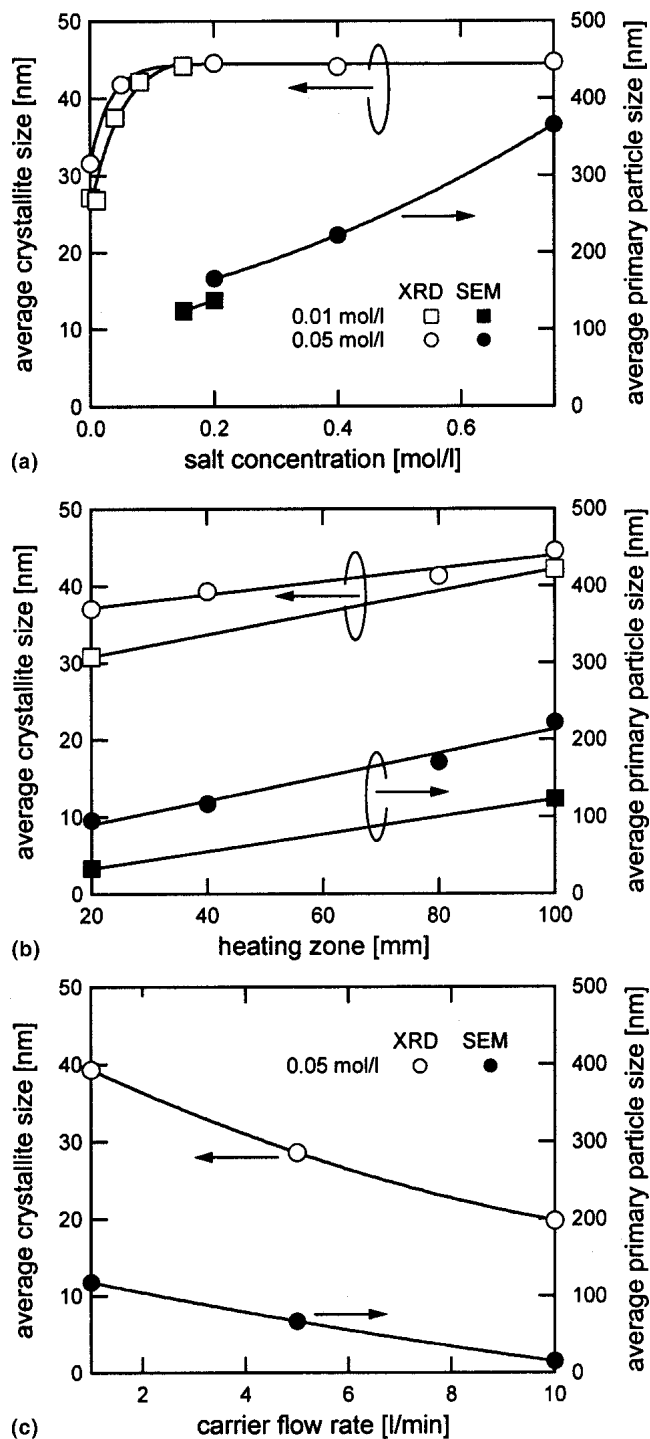
(a)

(b)

(c)

FIG. 8. Crystallite and primary particle size of BaTiO$_3$ particles estimated by Scherer's formula (XRD) and FE-SEM, respectively, as a function of (a) salt concentration, (b) furnace heating length, and (c) carrier gas flow rate. Increasing the salt concentration or the particle residence time in the hot zone increases both particle sizes.

prevent the formation of hard aggregates. The insets in the Fig. 7 show SEM images of BaTiO$_3$ particles before and after washing. Before washing, the particles are surrounded by salt that is completely removed by washing.

Figure 8 shows average crystallite sizes of BaTiO$_3$ particles, as calculated by Scherer's formula as a function of salt concentration and precursor concentration, i.e., 0.01 mol/l and 0.05 mol/l [Fig. 8(a)] for a heating zone 100 cm long [Figs. 6(c) and 6(g)]. Moreover, the average primary particle size as estimated from FE-SEM is also plotted in Fig. 8. The crystallite size increased with a salt concentration of around 0.1 mol/l but no further growth took place at concentrations above 0.15 mol/l. Figure 8(b) shows that increasing the length of the heating zone increased the crystallite size, consistent with the SEM images shown in Figs. 6(a)–6(c). Figure 8(c) shows that increasing the carrier gas flow rate decreased the crystallite size for a 40-cm length heating zone. This suggests that the reduced droplet/particle residence time in hot zones prevented the growth of crystallites.

IV. CONCLUSIONS

The effect of salt concentration and droplet/particle residence time in hot zone on the morphology and crystallinity of BaTiO$_3$ particles prepared by SASP was investigated. Increasing the concentration of the salt (which is eventually removed by washing) leads to an increase in crystallite size and a smoother surface, and contributes to the formation of tetragonal BaTiO$_3$ powders at the same temperature. Increasing the residence time in the hot zone by either extending the length of the pyrolysis furnace or reducing the carrier gas flow rate also resulted in an increased crystallite size. A prolonged residence time in the hot zone facilitated crystal growth while increasing salt concentration appears to retard the nucleation of barium titanate crystals, thus enhancing crystal growth and the size of the crystals produced.

REFERENCES

1. M.Z.C. Hu, V. Kurian, E.A. Payzant, C.J. Rawn, and R.D. Hunt, Powder Technol. **110,** 2 (2000).
2. G. Arlt, D. Hennings, and G. Dewith, J. Appl. Phys. **58,** 1619 (1985).

3. Y. Sakabe, N. Wada, and Y. Hamaji, J. Korean Phys. Soc. **32,** s260 (1998).

4. K. Kajiyoshi, N. Ishizawa, and M. Yoshimura, J. Am. Ceram. Soc. **74,** 369 (1991).

5. P.K. Dutta and J.R. Gregg, Chem. Mater. **4,** 843 (1992).

6. W.S. Cho, E. Hamada, and K. Takayanagi, J. Appl. Phys. **81,** 3000 (1997).

7. G.J. Choi, S.K. Lee, K.J. Woo, K.K. Koo, and Y.S. Cho, Chem. Mater. **10,** 4104 (1998).

8. L.B. Kong, J. Ma, R.F. Zhang, and W.X. Que, J. Alloys Compd. **337,** 226 (2002).

9. H. Xu, L. Gao, and J. Guo, J. Eur. Ceram. Soc. **22,** 1163 (2002).

10. S.W. Lu, B.I. Lee, Z.L. Wang, and W.D. Samuels, J. Cryst. Growth **219,** 269 (2000).

11. J.A. Kerchner, J. Moon, R.E. Chodelka, A.A. Morreone, and J.H. Adair, ACS Symp. Ser. **681,** 106 (1998).

12. O.B. Milosevic, M.K. Mirkovic, and D.P. Uskokovic, J. Am. Ceram. Soc. **79,** 1720 (1996).

13. T. Ogihara, H. Aikiyo, N. Ogata, and N. Mizutani, Adv. Powder Technol. **10,** 37 (1999).

14. K. Nonaka, S. Hayashi, K. Okada, and N. Otsuka, J. Mater. Res. **6,** 1750 (1991).

15. W. Maison, R. Kleeberg, R.B. Heimann, and S. Phanichphant, J. Eur. Ceram. Soc. **23,** 127 (2003).

16. B. Xia, I.W. Lenggoro, and K. Okuyama, Adv. Mater. **13,** 1579 (2001).

17. B. Xia, I.W. Lenggoro, and K. Okuyama, J. Mater. Chem. **13,** 2925 (2001).

18. B. Xia, I.W. Lenggoro, and K. Okuyama, Chem. Mater. **14,** 2623 (2002).

19. JCPDS File No. 31-174, Joint Committee for Powder Diffraction Standards, Newton Square, PA (1984).

20. ICDD. File No. 5-626, International Center for Diffraction Data, Newton Square, PA (1984).